ISSN 0915-633X

NATIONAL INSTITUTE FOR FUSION SCIENCE

Topological Transformations in Isolated Straight Magnetic Flux Tube

S. Bazdenkov, T. Sato and The Complexity Simulation Group

(Received - Feb. 17, 1997)

NIFS-486 Mar. 1997

RESEARCH REPORT
NIFS Series

This report was prepared as a preprint of work performed as a collaboration research of the National Institute for Fusion Science (NIFS) of Japan. This document is intended for information only and for future publication in a journal after some rearrangements of its contents.

Inquiries about copyright and reproduction should be addressed to the Research Information Center, National Institute for Fusion Science, Nagoya 464-01, Japan.

NAGOYA, JAPAN

TOPOLOGICAL TRANSFORMATIONS IN ISOLATED STRAIGHT MAGNETIC FLUX TUBE.

S.Bazdenkov, T.Sato and The Complexity Simulation Group[1]

Theory and Computer Simulation Center

National Institute for Fusion Science, Nagoya 464-01, Japan

Abstract

Reconnection in isolated straight magnetic flux tube with all the field lines continuosly twisted is investigated by a three-dimensional magnetohydrodynamic simulation. It is found that in the case of straight geometry drastic topological changes and prominent burst-like thermal energy release occur, even though no ambient untwisted magnetic field exists. Three distinct phases of the magnetic reconnection are observed. The first one corresponds to rapid (in the Alfven transit time-scale) kinking and split of the only initial flux tube into two topologically distinct well-bundled helical tubes. At the second phase these tubes rapidly reconnect each other in such a way that the configuration "turns inside out", i.e., each of the tubes, being compactly bundled at its one end, scatters to a thin shell surrounding another tube at the opposite end. During the third phase, the magnetic configuration becomes essentially knotted and topologically uncertain, but the knots are then rapidly kicked off by reconnection with further recurrence of two well-bundled tubes observed just after the split phase. A new feature of the magnetic reconnection associated with a double layer fine structure of reconnecting electric current is also observed in the simulation.

Keywords: magnetic reconnection, kink instability, coronal loop.

---

[1]K.Watanabe, R.Horiuchi, T.Hayashi, Y.Todo, A.Kageyama, T.H.Watanabe and H.Takamaru

I. INTRODUCTION

It is known that photospheric footpoint motions of the coronal magnetic field lines play a fundamental role in solar activity. The photospheric flows twist the coronal magnetic flux tubes and induce electric currents in the corona. When the tube is sufficiently twisted and electric current exceeds a threshold value, magnetic configuration becomes unstable to kink mode. As a result of kink instability, free magnetic energy is converted to kinetic and thermal plasma energies in fast time scale, and this is, probably, the main mechanism of coronal heating (Gold 1964; Parker 1972; Tucker 1973; Levine 1974; Rosner et al. 1978; Priest 1982). An important feature of this scenario is that the observed coronal heating can be satisfactorily explained by Joule dissipation only if the electric current is strongly concentrated into thin layers and, hence, is considerably enhanced in comparison with its homogeneous, within a flux tube, diffusive spatial distribution. Such a fine magnetic structure is believed to be created self-consistently during the evolution of kink instability, although there is an issue whether kinking, as itself, occurs in realistic coronal magnetic field or not (in the true coronal geometry the field is free to expand upward, so that its twist can relax gradually; see e.g. van Ballegooijen 1985). Hence, the coronal plasma dynamical response to photospheric twisting motions is of significant interest for solar physics. It has been studied by many authors (see, e.g. Strauss & Otani 1988; van Ballegooijen 1988; Biskamp & Welter 1989; Mikič et al. 1989; Mikič 1990; Dahlburg et al. 1991; Kusano et al. 1994; Van Hoven et al. 1995) using different geometries of the problem, differnet boundary conditions and various ranges of plasma parameters. The results of these studies, in general, agree with mentioned above scenario of the flux tube evolution, although some important detailes still need further investigation.

Recent numerical simulations by Amo et al. 1995 and Ozaki et al. 1997 put forward

the question about the necessity of an ambient untwisted magnetic field for an effective magnetic reconnection. According to these simulations, large energy release and drastic topological change in continuously twisted flux tube can be satisfactorily explained only if one takes overlying flux (ambient magnetic field) into account like an emerging flux model.

In the paper by Amo et al. 1995 (hereafter "A" model), evolution of braided magnetic field between two parallel superconducting planes is considered. Initially all the magnetic field lines (m.f.l.) of uniform magnetic field are assumed to be straight, but later some of them are twisted due to prescribed circular motion of their footpoints at the boundary planes. This motion is applied only within a localized region, so that there exist both twisted and untwisted m.f.l. which represent the flux tube as itself and the overlying flux, respectively. When the tube suffers considerable kink-like deformation, the twisted and untwisted m.f.l. come to closer contact and reconnect each other with consequent change in topology of magnetic configuration and significant release of magnetic energy.

In contrast, simulation by Ozaki et al. 1997 (hereafter "O" model) of a single coronal magnetic loop with all the m.f.l. twisted shows no such a drastic changes resulting from magnetic reconnection. In this model, initial current-free (i.e., potential) bipolar magnetic field emerges from two "holes" located in the same superconducting plane. These "holes" also represent the photospheric convective cells where the footpoints of all the m.f.l. are continuously twisted, so that there are no untwisted m.f.l. (i.e., overlying flux) in the system. The twisting motion induces electric current which, in turn, causes an upward expansion and stretching of the loop because of the hoop force. The hoop, probably, prevents global large-scale kink deformation of the loop, although an "internal" kink-like deformation certainly occurs inside the loop, so that its magnetic flux becomes turned in-

side out. Such a topological transformation, however, is not accompanied by considerable burst-like release of magnetic energy.

Thus, although kink instability develops in both the configurations "A" and "O", there is a considerable difference in the resulting energy release and other flare-like features of the flux tube evolution, which can be, probably, explained by the difference in the character of interaction between twisted and untwisted field lines in these configurations. However, there also exists a difference in the problem's geometry in "A" and "O" models which can affect the results irrespective of the ambient magnetic field (say, an upward expansion and stretching of a single loop can just reduce its free magnetic energy and wash away all the singularities in evolution of magnetic configuration). Hence, it is meaningful to separate the roles played by geometrical effects (i.e., the hoop) and overlying untwisted magnetic field. This motivated us to consider "mixed" model incorporating the following features of the "A" and "O" models: i) straight geometry of braided magnetic field, which excludes the hoop effect, as in "A" model; and ii) absence of an ambient untwisted magnetic field, when all the m.f.l. are twisted, like it takes place in the "O" model. In the "mixed" model, the initial current-free magnetic field emerges from two relatively small "holes" located in the top and the bottom superconducting boundary planes, and slow differential rotation is applied inside each of the "holes" as a boundary condition (see Fig.1). We also take the governing equations and all the plasma parameters to be the same as in simulation by Amo et al. 1995, so that any physically valuable difference in the obtained results should indicate directly the importance of interactions between twisted and untwisted m.f.l. in flare-like phenomena.

Another issue, considered in the present paper, concerns the details of magnetic reconnection driven by a kink-like deformation of continuously twisted flux tube. Using

a proper visualization technique, we investigate the generation of a small scale length magnetic structures (current layers) and topological transformations in three dimensional magnetic configuration.

The paper is organized as follows. In Sec.2 basic equations and simulation model are described. In Sec.3 the results of numerical simulation are presented. The conclusions are summarized in Sec.4.

2. THE MODEL.

We investigate MHD evolution of slightly dissipative three-dimensional plasma flow with the velocity $\mathbf{V}$ and magnetic field $\mathbf{B}$ which obey the set of MHD equations for low-β plasma:

$$\frac{\partial \mathbf{B}}{\partial \tau} = rot([\mathbf{V} \times \mathbf{B}] - \eta \mathbf{J}), \tag{1}$$

$$\frac{\partial \mathbf{V}}{\partial \tau} + (\mathbf{V} \cdot \nabla)\mathbf{V} = [\mathbf{J} \times \mathbf{B}] + \nu \Delta \mathbf{V}. \tag{2}$$

Here $\mathbf{J} \equiv rot\mathbf{B}$ is the normalized electric current density. In Eqs.(1),(2), magnetic field $\mathbf{B}$ is normalized by its characteristic value B_0 related with a total magnetic flux in the system (its value will be specified later). Dimensionless velocity field $\mathbf{V}$ is normalized by the Alfven velocity $V_A = \frac{B_0}{\sqrt{4\pi\rho}}$, where ρ is the initial plasma density. Spatial coordinates x, y, z are normalized by the distance L between the boundary planes of a cubic simulation domain, so that the boundaries are placed at $x = \pm\frac{1}{2}$, $y = \pm\frac{1}{2}$ and $z = 0; 1$ (see Fig.1). The dimensionless time τ is measured by corresponding transit Alfven time $t_A = \frac{L}{V_A}$.

In our simulation, the dimensionless plasma resistivity, η, and viscosity, ν, are taken to be constant and equal to 10^{-4} and 10^{-3}, respectively. In the case of plasma flow velocity of about $V \sim 10^{-1}$, which is typical for the simulation results presented in this paper, such a choice of the η and ν values corresponds to low-dissipation limit even in the range of small, about grid size, scale length.

The Eqs.(1),(2) correspond to low-β plasma limit when thermal energy converted from the magnetic and flow energies is expected to be immediately released by radiation, thermal conductivity or other processes. As the result, the effect of plasma pressure gradient becomes negligible in comparison with the pondermotive force $[\mathbf{J} \times \mathbf{B}]$ in the momentum equation (2). This situation is quite natural in many cases of the space and laboratory plasmas.

The momentum equation (2) does not guarantee that the plasma flow is always imcompressible, i.e., $div\mathbf{V} = 0$. Nevertheless, we assume the plasma density ρ to be uniform and constant, for the sake of simplicity. After the neglect of pressure term in Eq.(2), plasma density ρ appears only in the pondermotive acceleration term, as a multiplier, and plays no qualitatively important role.

Initially, at the time moment $\tau = 0$, plasma is assumed to be at rest:

$$\mathbf{V}\mid_{\tau=0} = 0. \tag{3}$$

Initial magnetic field $\mathbf{B}_0$ is taken to be a current-free potential field with the footpoints of all the m.f.l. concentrated within two "holes" of radius r_h in the boundary planes $z = 0$ and $z = 1$ (see Fig.1). Thus,

$$\mathbf{B}_0 = \nabla\alpha, \tag{4}$$

where the "potential" α is a solution to the problem

$$\Delta\alpha \equiv (\frac{\partial^2}{\partial x^2} + \frac{\partial^2}{\partial y^2} + \frac{\partial^2}{\partial z^2})\alpha = 0 \tag{5}$$

with the boundary condition that the normal component of magnetic field at the boundary is fixed to be equal to zero everywhere besides the "holes", where the nonzero magnetic flux emerges:

$$(\mathbf{n} \cdot \mathbf{B}_0) \mid_{hole} = B_{z0}(r). \tag{6}$$

Here r is the radial coordinate in the "hole" ($r \leq r_h$) and $\mathbf{n}$ is a unit vector normal to the boundary. The profile $B_{z0}(r)$ is chosen in a simplest way: $B_{z0}(r) = B_{zh} = constant$ for $r \leq (r_h - \varepsilon)$ and smoothly drops to zero inside thin peripheral layer, $(r_h - \varepsilon) \leq r \leq r_h$, with $\varepsilon \ll r_h$. The corresponding magnetic flux ψ , that emerges in the "hole", is approximately equal to $\psi \approx \pi r_h^2 B_{zh}$. Aiming to compare with the results of the "A" model, we chose the same magnetic flux value, $\psi = \psi_A = B_0 \cdot 1^2$, so that $B_{zh} \approx B_0 \frac{1}{\pi r_h^2}$ (note that r_h is the dimensionless radius of the "hole" which equals to 0.1 in the described simulation). Solving Eqs.(5),(6) with such a profile function $B_{z0}(r)$, we obtain initial magnetic field $\mathbf{B}_0$ which practically coinsides with the uniform initial field in "A" model everywhere besides relatively narrow layers near the boundary planes $z = 0$ and $z = 1$ (see Fig.2). In these layers, all the magnetic field lines are strongly bundled, so that their footpoints are concentrated within a "hole".

In our simulation, the boudaries are considered to be superconducting walls with no material transport allowed through them, i.e.,

$$\frac{\partial}{\partial \tau}(\mathbf{B} \cdot \mathbf{n})_{wall} = 0, \tag{7}$$

$$(\mathbf{V} \cdot \mathbf{n})_{wall} = 0, \tag{8}$$

where $\mathbf{n}$ is again a unit normal to the boundary plane. The tangential component of plasma flow velocity, as well, equals to zero everywhere in the boundary planes,

$$[\mathbf{V} \times \mathbf{n}] \mid_{wall} = 0, \tag{9}$$

besides the "holes" where circular motion is prescribed so as to twist continuously and steadily all the open m.f.l. in the system:

$$\mathbf{V} \mid_{z=0;1} = \pm V_{\vartheta 0}(r)\mathbf{e}_{\vartheta}. \tag{10}$$

Here $\mathbf{e}_{\vartheta}$ is an asimuthal unit vector of the cylindrical system of coordinates with the origin at $x = 0, y = 0$ at the corresponding boundary plane, and r is the radius. The twisting motion is concentrated inside a circular region of radius r_{twist}, so that the velocity profile $V_{\vartheta 0}(r)$ grows smoothly with r, reaches maximal value $V_{\vartheta 0} \mid_{max} = 0.1$ at $r = r_{twist} - \varepsilon$ and then smoothly drops to zero within the peripheral layer $r_{twist} - \varepsilon \leq r \leq r_{twist}$ (the details concerning twisting profile $V_{\vartheta 0}(r)$ can be found in Amo 1994). For each the "hole", a characteristic one-turn time T_{turn} is approximately equal to $2\pi \frac{r_{twist}}{V_{\vartheta 0} \mid_{max}} \approx 2\pi$ transit Alfven times. Hence, the flux tube is twisted in a slow adiabatic manner when the system has enough time to response and adjust its magnetic configuration.

In principle, the described geometry of the problem is characterized by the dimensionless parameter $\frac{r_{twist}}{r_h}$ whose value might play important role in establishment of different regimes of the flux tube evolution. In the present paper, however, we consider only the case when the "hole" and twisting zone are of the same size, $r_{twist} = r_h$, what is qualitatively sufficient for our purpose.

The governing Eqs.(1),(2) with the initial and boundary conditions Eqs.(3)-(10) have been solved numerically using a high precision MHD code developed by Sato & Hayashi

1979. The simulation box was implemented on a 101 × 101 × 101 grid point. A random noise with negligibly small amplitude was imposed on the initial configuration in order to provoke a further development of spatial modes. The twisting was started softly with a smooth transition from zero to a steady-state amplitude within a period of one transit Alfven time.

3. THE RESULTS.

We start with representing how the topology of three dimensional magnetic configuration changes in response to kink-like deformation of the flux tube with all the m.f.l. twisted. As a visualization technique, we employ the mapping generated by open magnetic field lines. Every open m.f.l. has always two footpoints, one of them located inside the bottom "hole" at the plane $z = 0$ and the other inside the top "hole" at the plane $z = 1$ (this is because of the boundary conditions Eqs.(6),(7) which fix the normal component of magnetic field at the superconducting boundary wall). Let (r, ϑ) and (R, Θ) be the cylindrical coordinates of the "top" and "bottom" footpoints of the same m.f.l.. Then the set of all the open m.f.l. gives the mapping $(r, \vartheta) \Longleftrightarrow (R, \Theta)$, i.e., an isomorphic point-to-point correspondence between the interiors of two "holes". In the case of an ideal plasma ($\eta = 0$), when all the m.f.l. are frozen into plasma flow, the only change in the mapping $(r, \vartheta) \Longleftrightarrow (R, \Theta)$, namely, the differential rotation, $\Theta = \vartheta + 2\tau V_{\vartheta 0}(r); R = r$, is due to applied "photospheric" vortex motions of the footpoints, Eq.(10), irrespective of the magnitude and complexity of the m.f.l. deformations between the boundary planes. However, in the plasma with finite resistivity, the magnetic field lines reconnect each other with corresponding footpoints "exchange", so that the described mapping is changed as well. Hence, temporal evolution of the mapping $(r, \vartheta) \Longleftrightarrow (R, \Theta)$ can serve as a diag-

nostics of magnetic reconnection and topological changes in magnetic configuration. In this paper, the mapping is calculated by tracing the set of 10^4 m.f.l.starting from the bottom "hole", and then it is visualized in such a way that the top footpoint of each m.f.l. with the coordinates $(R(r,\vartheta),\Theta(r,\vartheta))$ is colored depending on the location (r,ϑ) of its bottom counterpart. We chose a simple colormap $Color(r)$ which depends on the radius r only, so that the color runs from red to blue while the bottom footpoint radius r runs from zero to its near maximal value $0.9r_h$, and white color is prescribed for the "hole"'s periphery, $0.9r_h \le r \le r_h$.

In this way, temporal evolution of the "magnetic" mapping $(R(r,\vartheta),\Theta(r,\vartheta))$ is shown in Fig.3 where three distinct phases of magnetic reconnection are clearly seen (the numbers represent the dimensionless time moments).

First of all, no changes occur in the mapping during relatively long period of time, about $2.5T_{turn}$, when the magnetic configuration, being continuously twisted (the "total" twisting angle grows linearly, $\phi_{twist} = 2\tau$), remains stable until a kink instability develops there. This happens when the twist ϕ_{twist} exceeds a threshold value $\phi^*_{twist} \approx 4.8\pi$ which seems to be approximately the same for the flux tubes with different geometries (see, e.g. Mikič 1990 and the models "A" and "O"). The growth of kink-like deformation causes a "soft" but fast, within time interval $\frac{1}{10}T_{turn}$, split of the only initial flux tube into two, still well-bundled, tubes ("soft split" phase in Fig.3.a). Comparing the invading (white) and forced out (colored) magnetic fluxes in Fig.3.a, we have to conclude that the most part of the total initial magnetic flux ψ is reconnected in a fast time scale which is approximately 30 times smaller than the ordinary "diffusive" one. Thus, the observed split appears only as a result of driven magnetic reconnection with the rate everytime adjusted to and determined by the flow-induced perturbations of the magnetic configu-

ration. An important topological feature of the "soft split" phase is that the magnetic configuration, being initially characterized by the presence of topologically distinct "inner" and "outer" m.f.l., losses this property, so that every open m.f.l. has simultaneously both the "inner" and "outer" footpoints. Respectively, the "magnetic" mapping in Fig.3.a becomes symmetrical with respect to colored and white zones.

The second phase corresponds to rapid, within time interval of only $\frac{1}{20}T_{turn} \approx 0.3$, reconnection of the splitted well-bundled tubes in such a way that the magnetic configuration becomes "turned inside out" (see Fig.3.b). As a result, each of the tubes, being compactly bundled at its one end, scatters to a thin shell surrounding another tube at the opposite end, but this is a transitory structure. Actually, the bunch of m.f.l. scattered to a thin shell, promtly runs, as a result of magnetic reconnection (this is certainly not a physical flow), around the "hole" with the tendency to merge again at the opposite side, thus getting an additional twisting angle $\delta\phi \approx \pi$ within a time interval of about $\frac{1}{60}T_{turn} \approx 0.1$, i.e., immediately even in the transit Alfven time scale. This leap in the twist gives the origin of a future knot.

During the third phase of reconnection, magnetic configuration becomes essentially knotted (this will be clearly seen in Fig.4) and topologically uncertain (the "topological shock" phase in Fig.3.c). The chaotical component in the "magnetic" mapping arises because of an unstable tracing of the m.f.l. in the vicinity of an "essential" separatrix near would-be closing point of the knot. However, the knots are the transitory structures, as well, and they are rapidly kicked off by reconnection with further recurrence of the well-bundled flux tubes which remind the "splitted" structure in Fig.3.a, although reflected with "mirror" symmetry.

Temporal evolution of the knottedness is also shown in Fig.4.a,b where the snapshots

of the bunches of open m.f.l. are presented for the same phases of magnetic reconnection as in Fig.3.b,c. In Fig.4, green and red opaque objects are the bunches of m.f.l. starting from the central regions in the bottom and the top "holes", respectively (each of the bunches carries approximately 3 per cent of the total magnetic flux). The semi-transparent yellow object is the bunch of m.f.l. which starts around the red bunch in the top "hole" and carries about 10 per cent of the total magnetic flux.

So, an incipient knottedness arises immediately, within time interval $16.9 < \tau < 17.0$, as a result of magnetic reconnection near the "hole"'s periphery (see Fig.4.a and Fig.3.b). Then, within a middle time scale interval of about $\frac{1}{4}T_{turn} \approx \frac{\pi}{2}$, the knots develop and move towards the central plane $z = \frac{1}{2}$ in relatively quiet manner, without significant reconnection activity. During this period of time the magnetic configuration gets additional twist $\delta\phi \approx \pi$ because of the prescribed twisting motion at the boundaries. When the top and bottom knots meet each other near the central plane (see Fig.4.b, $19.0 \leq \tau \leq 19.2$), they are kicked off by magnetic reconnection in fast time scale of about $\frac{1}{20}T_{turn}$, and the configuration returns to familiar structure with two well-bundled tubes (compare Fig.4.b, $\tau = 19.6$ and Fig.4.a, $\tau = 16.7$). On the way to this recovered state, however, the system suffers a "topological shock" when the m.f.l. exhibit rather complicated behaviour.

In this respect, an interesting question arises about the generation of closed m.f.l. during the kicking off the knots (in Fig.4, only open m.f.l. are presented). One may expect that when the knot is cut off by reconnection, it can form, in principle, a separate toroidal structure wrapping the recovered bunch of the open m.f.l., as this is observed in Lau & Finn 1996. Of course, physically interesting set of closed m.f.l., which could be treated as the cut off knot, should carry magnetic energy comparable with the energy carried by open m.f.l. in the loop-like part of former knot. So, there is a sense in the

following procedure of checking whether the separated toroidal bunch of closed m.f.l. really exists or not. Namely, tracing the set of 10^4 open m.f.l., we distribute their starting points homogeneously inside the "hole" in such a way that each of the m.f.l. then represents a micro-flux tube with the magnetic flux $\delta\psi$ which is the same for all the traced m.f.l.. An "effective" local cross-section of the micro-tube is formally equal to $\frac{\delta\psi}{B}$, where B is local value of magnetic field. Respectively, the micro-tube's magnetic energy is $\delta W_m^{mt} = \int_{mfl} \frac{B^2}{2}\frac{\delta\psi}{B}\, dl = \frac{\delta\psi}{2}\int_{mfl} B\, dl$, hence, the total magnetic energy carried by all the open m.f.l. (micro-tubes) in the sytem is equal to $W_m^{mt} = \frac{\psi}{2}\sum\int_{mfl} B\, dl$ (here the integration is done along each of the traced m.f.l., and the sum is over all these m.f.l.). On the other hand, the total magnetic energy in the system is calculated directly by integration $W_m = \int_{cube} \frac{B^2}{2}\, d^3\mathbf{x}$ which, formally, takes into account all the field lines in the system. Hence, comparing these two quantities, one can find the magnetic energy carried by the structure with closed m.f.l. only. In our case, the difference $W_m^{open} = W_m - W_m^{mt}$ is less than few per cent of the total energy W_m, i.e., comparable with the numerical errors mostly arising as a result of coarse-grain division of the total magnetic flux ψ into 10^4 micro-tubes. This means that any set of closed m.f.l., if it exists, carries the "effective" magnetic flux $\psi^{open} \approx \frac{W_m^{open}}{B}$ much less than the flux involved into the topological transformations in Fig.4.b. and Fig.3.c.. Hence, it is unlikely that the knot, being cut off from the main bunch, forms a separated toroidal structure wrapping the recovered bunch. The knottedness seems to dissappear mostly due to reconnection of the open m.f.l. with each other.

Thus, the observed topological transformations occur in a short time scale and affect the most part of total magnetic flux in the system. Let us now consider the corresponding changes in system's energetics.

In Fig.5, temporal evolution of the energy consumption rate (curve 1), i.e., the Poynting flux through the boundaries, $P = \int_{walls}([\mathbf{B} \times [\mathbf{V} \times \mathbf{B}]] \cdot d\mathbf{S})$, and the rate of Joule dissipation (curve 2), $W_J = \eta \int_{cube} J^2 d^3\mathbf{x}$, is presented (time intervals I, II and III correspond to the phases of magnetic reconnection described above). As this is in the "A" model, the Poynting flux rapidly drops when the m.f.l. reconnect each other with corresponding decrease of their twist. Simultaneously, burst-like release of thermal energy, in the form of Joule heating, takes place. An important feature of this process is that the split, as itself, of the only initial flux tube into two tubes is not accompanied by any changes in system's energetics. Actually, both the rates P and W_J are considerably changed, about 30 per cent of their values just before the event, only during the fast "turn inside out" phase of magnetic reconnection. The absolute value of thermal energy release exceeds approximately twice the corresponding value observed in simulation by Amo et al. 1995, even though the magnetic field and plasma parameters are chosen to be the same in both the cases.

Topological transformations are also accompanied by the burst-like release and spatial redistribution of magnetic energy. This is seen in Fig.6 where the total magnetic energy (curve 1) and the magnetic energies inside (curve 2) and outside (curve 3) the twisting zone are shown. In the absolute value, energy release exceeds the observed one in the "A" model but, simultaneously, is negligible in comparison with total magnetic energy which is 100 times higher than in "A" case (this is a result of strong bundling and amplification of the magnetic field near the "holes"). Thus, the total magnetic energy is approximately constant, in the relative sense, during the rearrangement of the m.f.l.. However, there occurs considerable, even in the relative sense, burst-like magnetic energy exchange between different parts of the system (see curves 2 and 3 in Fig.6). An interesting feature of this

burst-like event is that the magnetic energy is redistributed from outer into inner part of magnetic configuration, what is just opposite to the "ordinary" interaction between twisted and untwisted m.f.l. in the model "A".

In our simulation, we also observe a new feature of magnetic reconnection associated with a double-layer fine structure of reconnecting electric current. Typical spatial distribution of an electric current density during the most active phase of magnetic reconnection (namely, for the time moment $\tau = 19.2$) is shown in Fig.7. Here the yellow and red isosurfaces of $\mid \mathbf{J} \mid \equiv \mid rot\mathbf{B} \mid = constant$ correspond to negative and positive values of the longitudinal component of electric current density, $\frac{(\mathbf{J} \cdot \mathbf{B})}{\mid \mathbf{B} \mid}$, respectively. It is clearly seen in Fig.7 that, besides the cylindrical column of the regular (negative) current induced by the prescribed twisting motion of the m.f.l. footpoints, there also exists a double current layer (red-and-yellow helical double stripe) with oppositely directed "singular" reconnecting currents. While all the m.f.l. in the system are twisted, no positive (red) regular current is induced directly. So, the observed reconnecting current (red stripe), which is opposite to the regular one, is generated only as a result of plasma motions during the evolution of kink instability. This current is accompanied by its "singular", i.e., strongly concentrated, oppositely directed counterpart (yellow stripe), and both the "singular" currents are approximately counter- and co-directed with respect to surrounding magnetic field. The magnetic field lines in the narrow space between current layers are near parallel but structurally divergent. This is seen in Fig.7, where the green object is the bunch of m.f.l. started in the lower part of the double layer interior. If, at the starting point, the bunch of m.f.l. is taken a little bit wider, then it becomes of very complicated form, like the m.f.l. in Fig.4.b.. So, with high probability, the reconnection activity is mostly concentrated inside this double layer structure.

This is also in agreement with Fig.8 where, in addition to the spatial distribution of electric current density, the same as in Fig.7, the distribution of plasma flow velocity is presented (green object is an isosurface of $\mid \mathbf{V} \mid = constant = 0.5$). An important feature of the flow is the existence of two intensive oppositely directed "flat" jets which dash out from the double current layer everywhere along the layer's side boundary. As the generation of intensive plasma jets in the vicinity of reconnection region is a generic feature of driven magnetic reconnection, we may conclude that the observed double current layer is really the region where the reconnection activity is concentrated.

Both the "singular" components of the double current layer have approximately the same absolute value and arise in the same time instant (see Fig.9), i.e., they are really the counterparts of the same compound structure.

4. CONCLUSIONS.

We have studied, by a three-dimensional MHD simulation, temporal evolution of isolated straight magnetic flux tube with all the m.f.l. continuously twisted. As the initial magnetic field, a current-free potential field emerging from two convection "holes" in the top and bottom superconducting boundary planes is given.

It is shown that in the case of "straight" geometry the twist causes kink instability with consequent generation of singular current layers and significant thermal energy release even in the absence of an ambient untwisted magnetic field. In this respect, physically important difference between the "straight" and "loop" ("O") geometries, both without an ambient untwisted magnetic field, is, probably, related with an upward expansion and stretching of the loop when all the singularities in plasma dynamics are essentially washed away.

Concerning the topological transformations in reconnecting kink, three qualitatively

distinct phases of magnetic reconnection are found: i) rapid split of the only initial flux tube into two wel-bundled tubes; ii) fast "turning inside out" of the magnetic configuration followed by the origin of incipient knottedness; and iii) the development and kicking off the knots with further recovering of the splitted well-bundled flux tubes. The topological transformations are accompanied by drastic changes in the system's energetics, especially at the second phase of reconnection. A new interesting feature of this process is that the significant "inverse" magnetic energy exchange between outer and inner parts of magnetic configuration occurs in a fast time scale while the total magnetic energy is approximately constant. Namely, the magnetic energy is considerably redistributed from outer into inner part of magnetic configuration, what is just opposite to the "ordinary" interaction between twisted and untwisted m.f.l..

Another interesting and new feature of magnetic reconnection, which is found in our simulation, concerns the double layer structure of reconnecting electric current. It is found that both the "singular" components of this structure (oppositely directed thin current stripes) have the same magnitude and arise at the same time moment, i.e., are really the counterparts of the same compound. The double current layer ejects two intensive "flat" jets which dash out everywhere along the layer's side boundary. As the generation of intensive plasma jets in the vicinity of reconnection region is a generic feature of driven magnetic reconnection, we may conclude that the observed double current layer is really the region where the reconnection activity is concentrated.

ACKNOWLEDGEMENT

This work was performed by using the Advanced Computing System for Complexity Simulation at NIFS under the support of Grants-in-Aid of the Ministry of Education, Science and Culture in Japan (No. 08226104, No. 08044109 and No. 07832024).

References

Amo H., Sato T., Kageyama A. and The Complexity Simulation Group, Phys.Rev. E, **51**, n.5, R3838 (1995).

Amo H., PhD Dissertation (1994).

Biskamp D. & Welter H., Solar Physics, **120**, 49 (1989).

Dahlburg R.B., Antiochos S.K. and Zang T.A., Ap.J., **383**, 420 (1991).

Gold T., in "The Physics of Solar Flares" (NASA SP-50), ed. W.Hess, p.389 (1964).

Kusano K., Suzuki Y., Kubo H., Miyoshi T. and Nishikawa K., Ap.J., **433**, 361 (1994).

Lau Y.-T. & Finn J.M., Phys. Plasmas, **3**, n.11, 3983 (1996).

Levine R.H., Ap.J., **190**, 457 (1974).

Mikič Z., Phys.Fluids B, 2, 1450 (1990).

Mikič Z., Schnack D.D. and Van Hoven G., Ap.J., **338**, 1148 (1989).

Ozaki M., Sato T. and Hayashi T., Ap.J., in print (1997).

Parker E.N., Ap.J., **174**, 499 (1972).

Priest E.R., "Solar Magnetohydrodynamics" (Dordrecht: Reidel), 1982.

Rosner R., Tucker W.H. and Vaiana G.S., Ap.J., **220**, 643 (1978).

Sato T. and Hayashi T., Phys.Fluids, **22**, 1189 (1979).

Strauss H., & Otani N., Ap.J., **326**, 418 (1988).

Tucker W.H., Ap.J., **186**, 285 (1973).

van Ballegooijen A.A., Ap.J., **298**, 421 (1985).

van Ballegooijen A.A., Geophys.Ap.Fluid Dyn., **41**, 181 (1988).

Van Hoven G., Mok Y. and Mikič Z., Ap.J., **440**, L105 (1995).

Figure Captions

Fig.1.- Geometry of the problem. Magnetic field emerges only inside the "holes" (shaded). Green object represents the bunch of m.f.l. (simulation result).

Fig.2.- Initial current-free magnetic field.

(a) - magnetic field lines in the $(z-x)$ plane (radial position of k-th footpoint in the "hole", r_k, is chosen as to represent the equidistant magnetic flux surfaces, i.e., $\delta\psi = 2\pi \int_{r_k}^{r_{k+1}} B_{z0}(r)\, r\, dr = constant = 0.1\psi$);

(b) - the z-component of $\mathbf{B}$ at the planes $z=0$ (plate), $z=\frac{1}{6}$ (marked), $z=\frac{1}{3}$ and $z=\frac{1}{2}$.

Fig.3.- Temporal evolution of the "magnetic" mapping which gives point-to-point correspondence between the top and bottom footpoints of 10^4 m.f.l.. Three phases of magnetic reconnection:

(a) - soft split;

(b) - turning inside out;

(c) - topological shock and recurrence.

Fig.4.- Temporal evolution of the bunches of m.f.l.:

(a) - appearance of an incipient knottedness;

(b) - topological shock.

Fig.5.- Temporal evolution of the Poynting flux (curve 1) and the rate of Joule dissipation (curve 2). The time intervals I, II and III correspond respectively to the phases (a), (b) and (c) in Fig.3.

Fig.6.- Burst-like spatial redistribution of magnetic energy during the reconnection: curve 1 - the total magnetic energy; curve 2 - magnetic energy inside twisting zone ($r \leq r_{twist}$); curve 3 - magnetic energy outside twisting zone.

Fig.7.- Thin double layer structure of reconnecting electric current at the time moment $\tau = 19.2$ (yellow and red objects are the isosurfaces of negative and positive longitudinal current density value; green object is the bunch of m.f.l. traced from a small circle inside the double layer).

Fig.8.- Intensive "flat" jets dashed out from the same double current layer as in Fig.7 (green object is the isosurface of plasma flow velocity which is about a half of local Alfven velocity and 5 times higher the maximal twisting velocity).

Fig.9.- Temporal evolution of the maximal and minimal current density values (actually, they correspond to electric current density values in the counterparts of the double current layer).

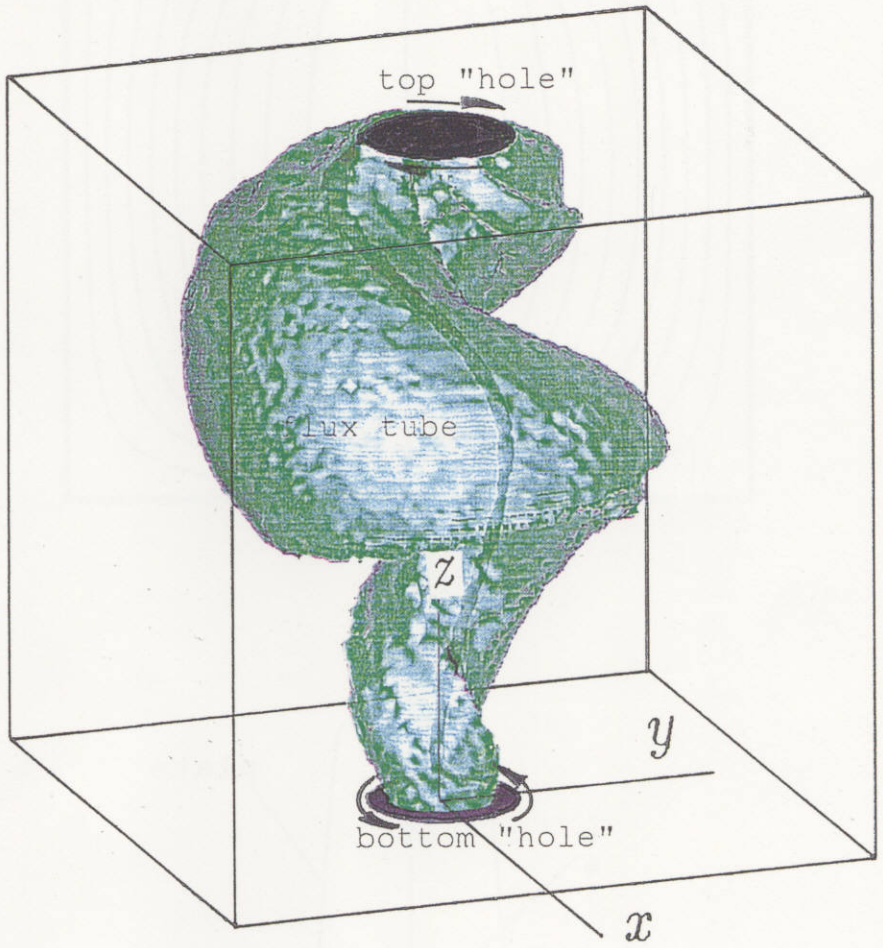

Fig.1.

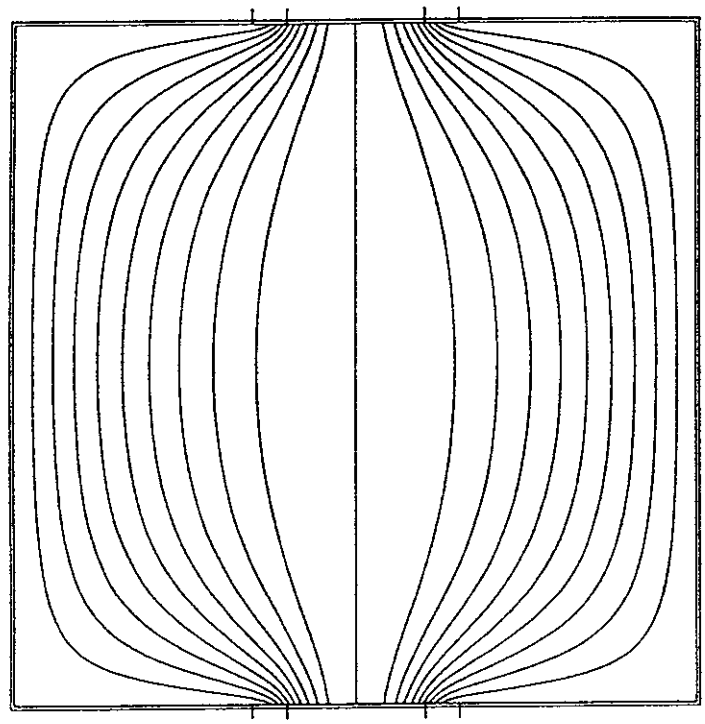

(a)

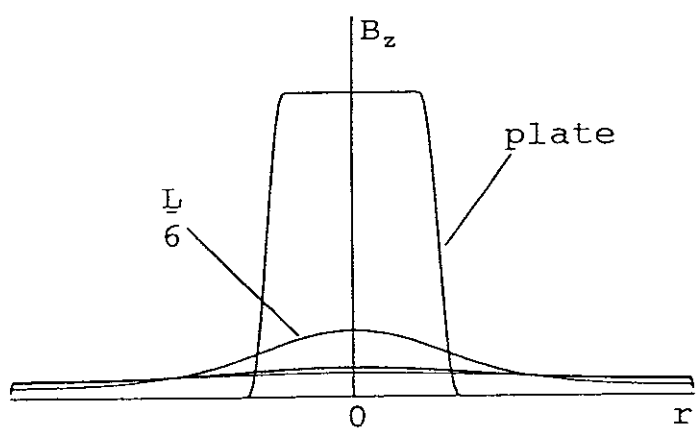

(b)

Fig.2

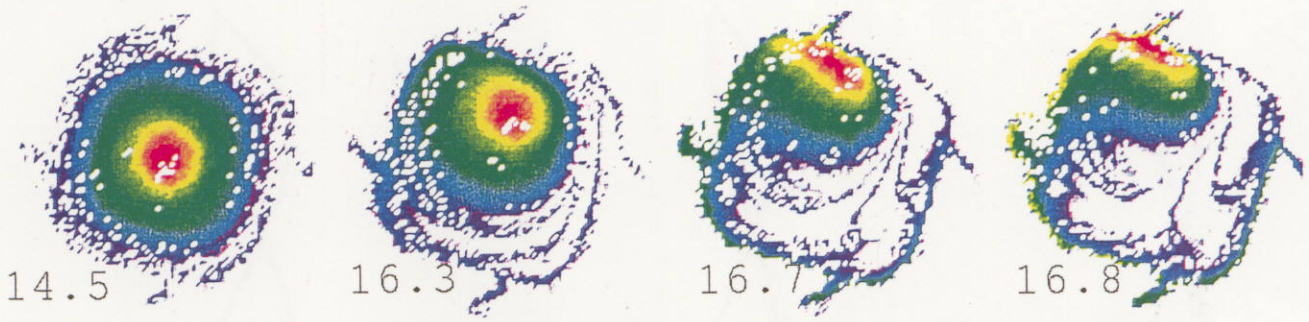

a) "soft split"

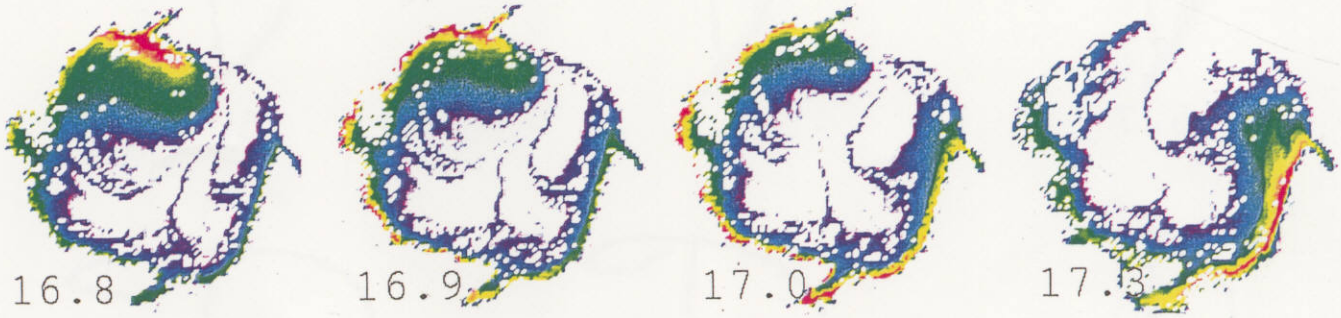

b) "turn inside out"

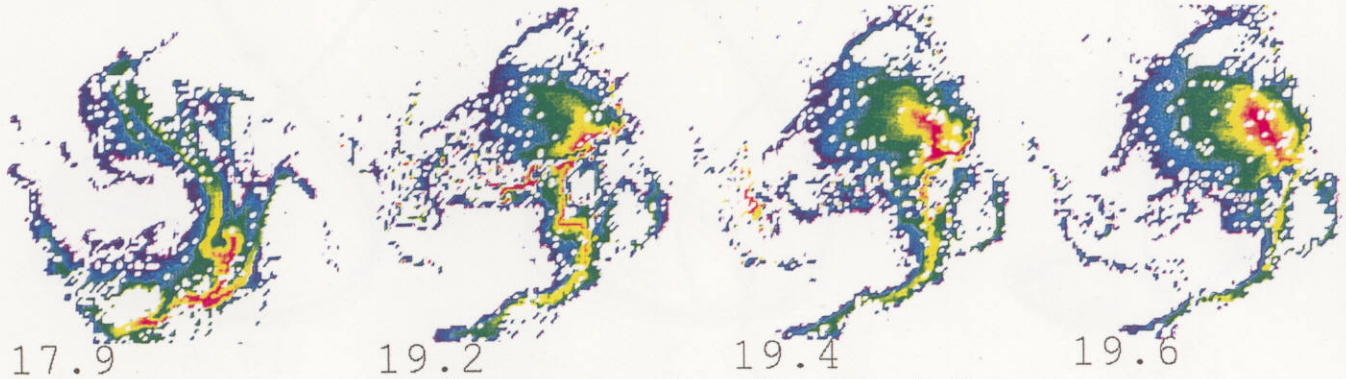

c) "topological shock"

Fig.3

16.7

16.8

16.9

17.0

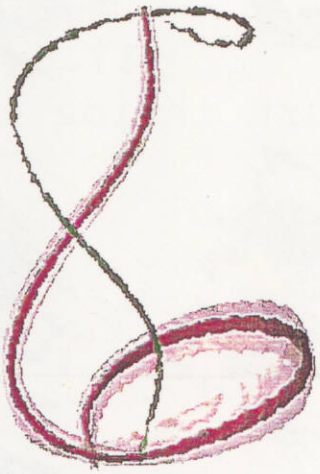

17.3

17.6

Fig.4.a

17.9

18.1

18.95

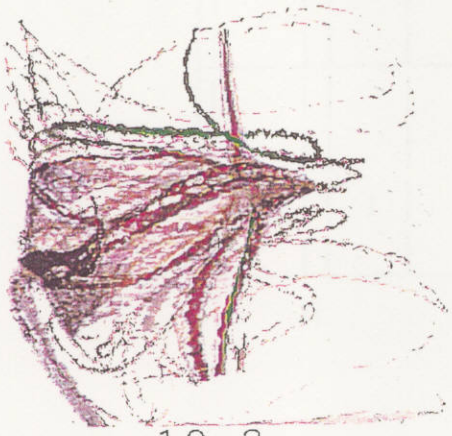

19.2

19.4

19.6

Fig.4.b

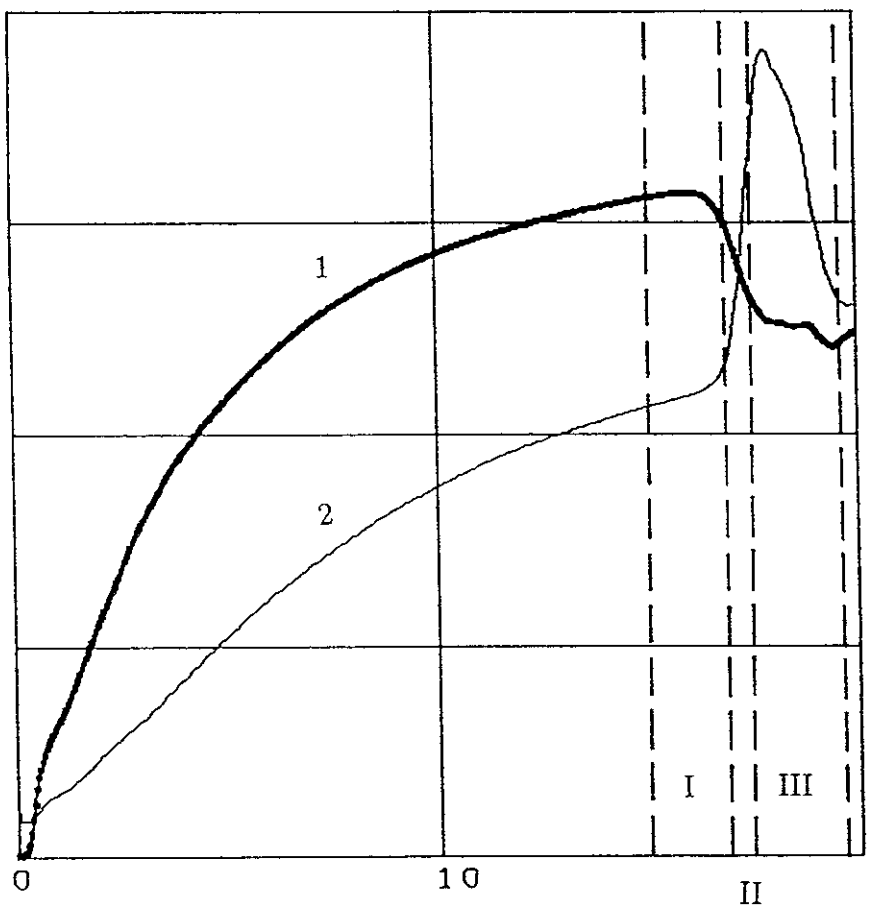

Fig.5

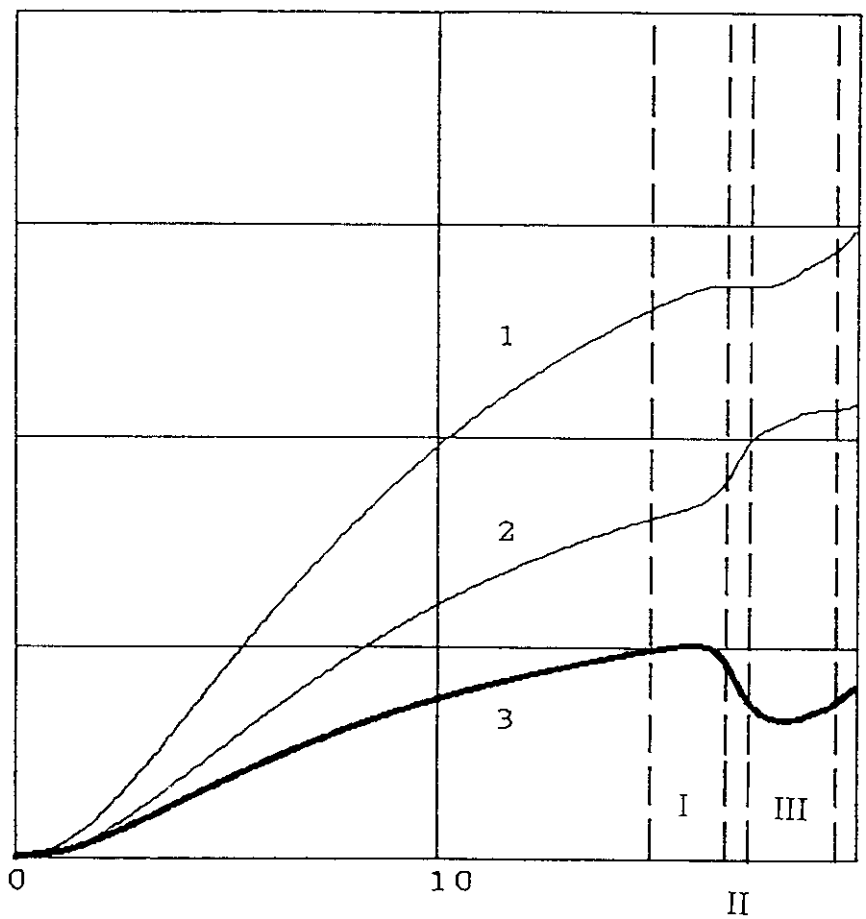

Fig.6

Fig.7

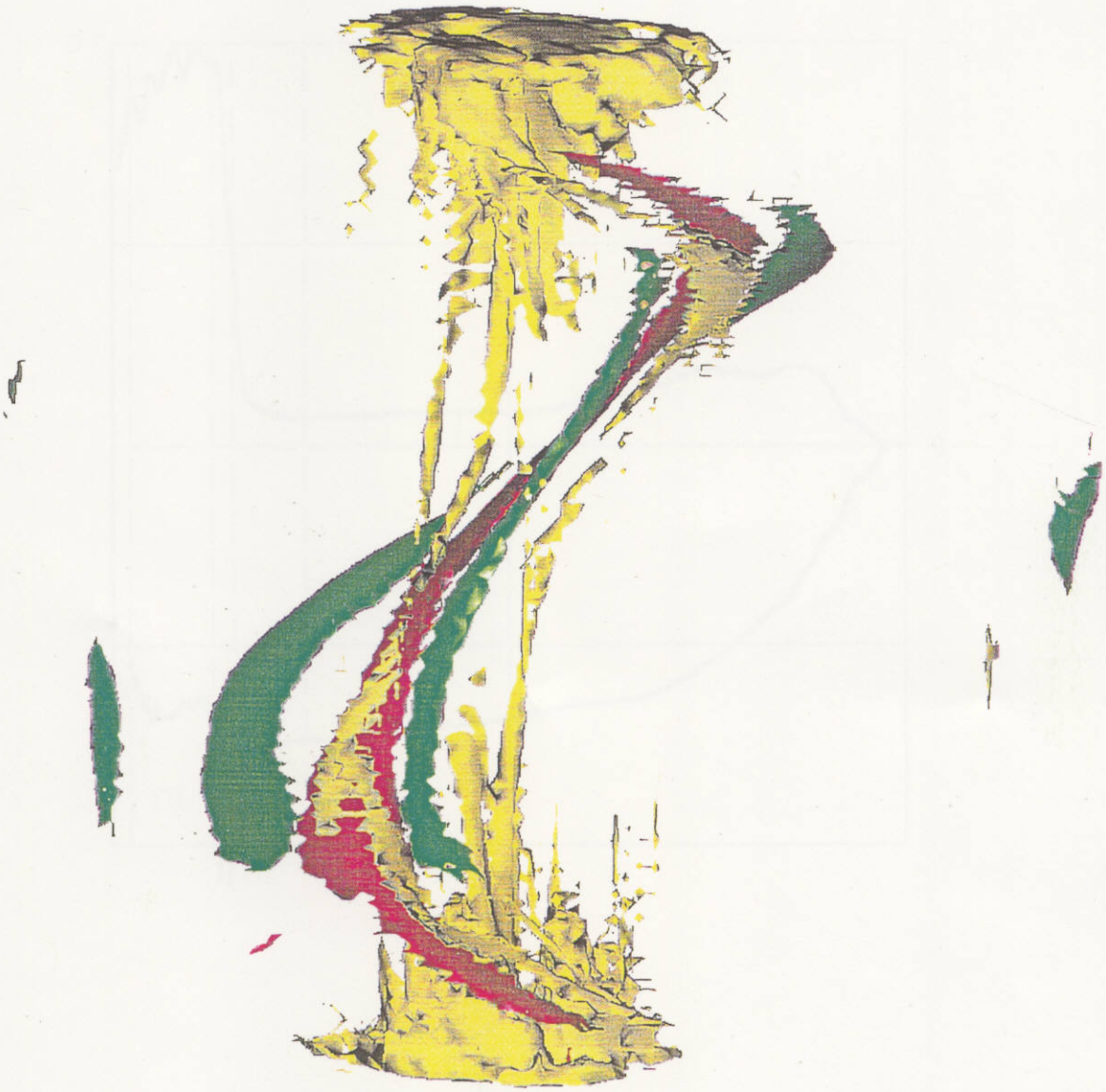

Fig.8

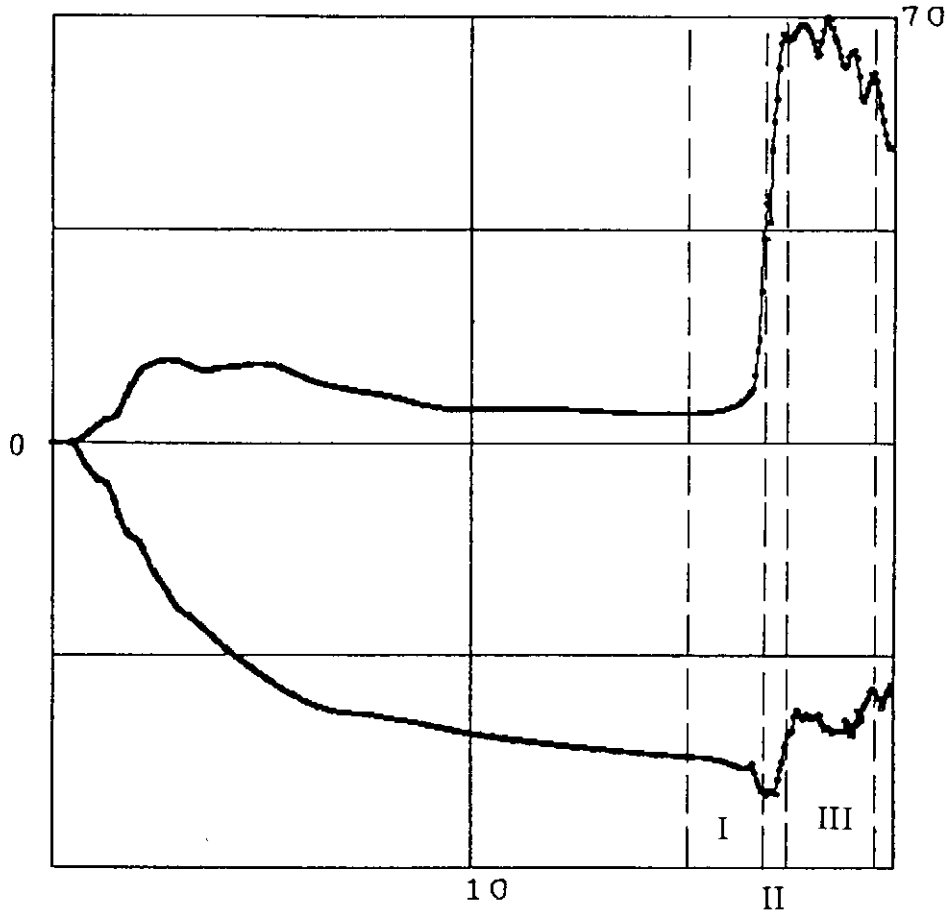

Fig.9

Recent Issues of NIFS Series

NIFS-443 Y. Todo, T. Sato and The Complexity Simulation Group,
Vlasov-MHD and Particle-MHD Simulations of the Toroidal Alfvén Eigenmode; Sep. 1996 (IAEA-CN-64/D2-3)

NIFS-444 A. Fujisawa, S. Kubo, H. Iguchi, H. Idei, T. Minami, H. Sanuki, K. Itoh, S. Okamura, K. Matsuoka, K. Tanaka, S. Lee, M. Kojima, T.P. Crowley, Y. Hamada, M. Iwase, H. Nagasaki, H. Suzuki, N. Inoue, R. Akiyama, M. Osakabe, S. Morita, C. Takahashi, S. Muto, A. Ejiri, K. Ida, S. Nishimura, K. Narihara, I. Yamada, K. Toi, S. Ohdachi, T. Ozaki, A. Komori, K. Nishimura, S. Hidekuma, K. Ohkubo, D.A. Rasmussen, J.B. Wilgen, M. Murakami, T. Watari and M. Fujiwara,
An Experimental Study of Plasma Confinement and Heating Efficiency through the Potential Profile Measurements with a Heavy Ion Beam Probe in the Compact Helical System; Sep. 1996 (IAEA-CN-64/C1-5)

NIFS-445 O. Motojima, N. Yanagi, S. Imagawa, K. Takahata, S. Yamada, A. Iwamoto, H. Chikaraishi, S. Kitagawa, R. Maekawa, S. Masuzaki, T. Mito, T. Morisaki, A. Nishimura, S. Sakakibara, S. Satoh, T. Satow, H. Tamura, S. Tanahashi, K. Watanabe, S. Yamaguchi, J. Yamamoto, M.Fujiwara and A. Iiyoshi,
Superconducting Magnet Design and Construction of LHD; Sep. 1996 (IAEA-CN-64/G2-4)

NIFS-446 S. Murakami, N. Nakajima, S. Okamura, M. Okamoto and U. Gasparino,
Orbit Effects of Energetic Particles on the Reachable β–Value and the Radial Electric Field in NBI and ECR Heated Heliotron Plasmas; Sep. 1996 (IAEA-CN-64/CP -6) Sep. 1996

NIFS-447 K. Yamazaki, A. Sagara, O. Motojima, M. Fujiwara, T. Amano, H. Chikaraishi, S. Imagawa, T. Muroga, N. Noda, N. Ohyabu, T. Satow, J.F. Wang, K.Y. Watanabe, J. Yamamoto . H. Yamanishi, A. Kohyama, H. Matsui, O. Mitarai, T. Noda, A.A. Shishkin, S. Tanaka and T. Terai
Design Assessment of Heliotron Reactor; Sep. 1996 (IAEA-CN-64/G1-5)

NIFS-448 M. Ozaki, T. Sato and the Complexity Simulation Group,
Interactions of Convecting Magnetic Loops and Arcades; Sep. 1996

NIFS-449 T. Aoki,
Interpolated Differential Operator (IDO) Scheme for Solving Partial Differential Equations; Sep. 1996

NIFS-450 D. Biskamp and T. Sato,
Partial Reconnection in the Sawtooth Collapse; Sep. 1996

NIFS-451 J. Li, X. Gong, L. Luo, F.X. Yin, N. Noda, B. Wan, W. Xu, X. Gao, F. Yin, J.G. Jiang, Z. Wu., J.Y. Zhao, M. Wu, S. Liu and Y. Han,
Effects of High Z Probe on Plasma Behavior in HT-6M Tokamak; Sep. 1996

NIFS-452 N. Nakajima, K. Ichiguchi, M. Okamoto and R.L. Dewar,

Ballooning Modes in Heliotrons/Torsatrons; Sep. 1996 (IAEA-CN-64/D3-6)

NIFS-453 A. Iiyoshi,
Overview of Helical Systems; Sep. 1996 (IAEA-CN-64/O1-7)

NIFS-454 S. Saito, Y. Nomura, K. Hirose and Y.H. Ichikawa,
Separatrix Reconnection and Periodic Orbit Annihilation in the Harper Map; Oct. 1996

NIFS-455 K. Ichiguchi, N. Nakajima and M. Okamoto,
Topics on MHD Equilibrium and Stability in Heliotron / Torsatron; Oct. 1996

NIFS-456 G. Kawahara, S. Kida, M. Tanaka and S. Yanase,
Wrap, Tilt and Stretch of Vorticity Lines around a Strong Straight Vortex Tube in a Simple Shear Flow; Oct. 1996

NIFS-457 K. Itoh, S.- I. Itoh, A. Fukuyama and M. Yagi,
Turbulent Transport and Structural Transition in Confined Plasmas; Oct. 1996

NIFS-458 A. Kageyama and T. Sato,
Generation Mechanism of a Dipole Field by a Magnetohydrodynamic Dynamo; Oct. 1996

NIFS-459 K. Araki, J. Mizushima and S. Yanase,
The Non-axisymmetric Instability of the Wide-Gap Spherical Couette Flow; Oct. 1996

NIFS-460 Y. Hamada, A. Fujisawa, H. Iguchi, A. Nishizawa and Y. Kawasumi,
A Tandem Parallel Plate Analyzer; Nov. 1996

NIFS-461 Y. Hamada, A. Nishizawa, Y. Kawasumi, A. Fujisawa, K. Narihara, K. Ida, A. Ejiri, S. Ohdachi, K. Kawahata, K. Toi, K. Sato, T. Seki, H. Iguchi, K. Adachi, S. Hidekuma, S.Hirokura, K. Iwasaki, T. Ido, M. Kojima, J. Koong, R. Kumazawa, H. Kuramoto, T. Minami, I. Nomura, H. Sakakita, M. Sasao, K.N. Sato, T. Tsuzuki, J. Xu, I. Yamada and T. Watari,
Density Fluctuation in JIPP T-IIU Tokamak Plasmas Measured by a Heavy Ion Beam Probe; Nov. 1996

NIFS-462 N. Katsuragawa, H. Hojo and A. Mase,
Simulation Study on Cross Polarization Scattering of Ultrashort-Pulse Electromagnetic Waves; Nov. 1996

NIFS-463 V. Voitsenya, V. Konovalov, O. Motojima, K. Narihara, M. Becker and B. Schunke,
Evaluations of Different Metals for Manufacturing Mirrors of Thomson Scattering System for the LHD Divertor Plasma; Nov. 1996

NIFS-464 M. Pereyaslavets, M. Sato, T. Shimozuma, Y. Takita, H. Idei, S. Kubo, K. Ohkubo and K. Hayashi,

Development and Simulation of RF Components for High Power Millimeter Wave Gyrotrons; Nov. 1996

NIFS-465 V.S. Voitsenya, S. Masuzaki, O. Motojima, N. Noda and N. Ohyabu,
On the Use of CX Atom Analyzer for Study Characteristics of Ion Component in a LHD Divertor Plasma; Dec. 1996

NIFS-466 H. Miura and S. Kida,
Identification of Tubular Vortices in Complex Flows; Dec. 1996

NIFS-467 Y. Takeiri, Y. Oka, M. Osakabe, K. Tsumori, O. Kaneko, T. Takanashi, E. Asano, T. Kawamoto, R. Akiyama and T. Kuroda,
Suppression of Accelerated Electrons in a High-current Large Negative Ion Source; Dec. 1996

NIFS-468 A. Sagara, Y. Hasegawa, K. Tsuzuki, N. Inoue, H. Suzuki, T. Morisaki, N. Noda, O. Motojima, S. Okamura, K. Matsuoka, R. Akiyama, K. Ida, H. Idei, K. Iwasaki, S. Kubo, T. Minami, S. Morita, K. Narihara, T. Ozaki, K. Sato, C. Takahashi, K. Tanaka, K. Toi and I. Yamada,
Real Time Boronization Experiments in CHS and Scaling for LHD; Dec. 1996

NIFS-469 V.L. Vdovin, T.Watari and A. Fukuyama,
3D Maxwell-Vlasov Boundary Value Problem Solution in Stellarator Geometry in Ion Cyclotron Frequency Range (final report); Dec. 1996

NIFS-470 N. Nakajima, M. Yokoyama, M. Okamoto and J. Nührenberg,
Optimization of M=2 Stellarator; Dec. 1996

NIFS-471 A. Fujisawa, H. Iguchi, S. Lee and Y. Hamada,
Effects of Horizontal Injection Angle Displacements on Energy Measurements with Parallel Plate Energy Analyzer; Dec. 1996

NIFS-472 R. Kanno, N. Nakajima, H. Sugama, M. Okamoto and Y. Ogawa,
Effects of Finite-β and Radial Electric Fields on Neoclassical Transport in the Large Helical Device; Jan. 1997

NIFS-473 S. Murakami, N. Nakajima, U. Gasparino and M. Okamoto,
Simulation Study of Radial Electric Field in CHS and LHD; Jan. 1997

NIFS-474 K. Ohkubo, S. Kubo, H. Idei, M. Sato, T. Shimozuma and Y. Takita,
Coupling of Tilting Gaussian Beam with Hybrid Mode in the Corrugated Waveguide; Jan. 1997

NIFS-475 A. Fujisawa, H. Iguchi, S. Lee and Y. Hamada,
Consideration of Fluctuation in Secondary Beam Intensity of Heavy Ion Beam Prove Measurements; Jan. 1997

NIFS-476 Y. Takeiri, M. Osakabe, Y. Oka, K. Tsumori. O. Kaneko. T. Takanashi, E. Asano, T. Kawamoto, R. Akiyama and T. Kuroda,

Long-pulse Operation of a Cesium-Seeded High-Current Large Negative Ion Source; Jan. 1997

NIFS-477 H. Kuramoto, K. Toi, N. Haraki, K. Sato, J. Xu, A. Ejiri, K. Narihara, T. Seki, S. Ohdachi, K. Adati, R. Akiyama, Y. Hamada, S. Hirokura, K. Kawahata and M. Kojima,
Study of Toroidal Current Penetration during Current Ramp in JIPP T-IIU with Fast Response Zeeman Polarimeter; Jan., 1997

NIFS-478 H. Sugama and W. Horton,
Neoclassical Electron and Ion Transport in Toroidally Rotating Plasmas; Jan. 1997

NIFS-479 V.L. Vdovin and I.V. Kamenskij,
3D Electromagnetic Theory of ICRF Multi Port Multi Loop Antenna; Jan. 1997

NIFS-480 W.X. Wang, M. Okamoto, N. Nakajima, S Murakami and N. Ohyabu,
Cooling Effect of Secondary Electrons in the High Temperature Divertor Operation; Feb. 1997

NIFS-481 K. Itoh. S.-I. Itoh, H. Soltwisch and H.R. Koslowski,
Generation of Toroidal Current Sheet at Sawtooth Crash; Feb. 1997

NIFS-482 K. Ichiguchi,
Collisionality Dependence of Mercier Stability in LHD Equilibria with Bootstrap Currents; Feb. 1997

NIFS-483 S. Fujiwara and T. Sato,
Molecular Dynamics Simulations of Structural Formation of a Single Polymer Chain: Bond-orientational Order and Conformational Defects; Feb. 1997

NIFS-484 T. Ohkawa,
Reduction of Turbulence by Sheared Toroidal Flow on a Flux Surface; Feb. 1997

NIFS-485 K. Narihara, K. Toi, Y. Hamada, K. Yamauchi, K. Adachi, I. Yamada, K. N. Sato, K. Kawahata, A. Nishizawa, S. Ohdachi, K. Sato, T. Seki, T. Watari, J. Xu, A. Ejiri, S. Hirokura, K. Ida, Y. Kawasumi, M. Kojima, H. Sakakita, T. Ido, K. Kitachi, J. Koog and H. Kuramoto,
Observation of Dusts by Laser Scattering Method in theJIPPT-IIU Tokamak Mar. 1997

NIFS-486 S. Bazdenkov, T. Sato and The Complexity Simulation Group,
Topological Transformations in Isolated Straight Magnetic Flux Tube; Mar. 1997